Systematic analysis of differential rhythmic liver gene expression mediated by the circadian clock and feeding rhythms

Benjamin D. Weger[a,b,c], Cédric Gobet[a,b], Fabrice P. A. David[b,d,e], Florian Atger[a,f,1], Eva Martin[a,2], Nicholas E. Phillips[b], Aline Charpagne[a,3], Meltem Weger[c], Felix Naef[b,4], and Frédéric Gachon[a,b,c,4]

[a]Société des Produits Nestlé, Nestlé Research, CH-1015 Lausanne, Switzerland; [b]Institute of Bioengineering, School of Life Sciences, Ecole Polytechnique Fédérale de Lausanne, CH-1015 Lausanne, Switzerland; [c]Institute for Molecular Bioscience, The University of Queensland, St. Lucia QLD-4072, Australia; [d]Gene Expression Core Facility, Ecole Polytechnique Fédérale de Lausanne, CH-1015 Lausanne, Switzerland; [e]BioInformatics Competence Center, Ecole Polytechnique Fédérale de Lausanne, CH-1015 Lausanne, Switzerland; and [f]Department of Pharmacology and Toxicology, University of Lausanne, CH-1015 Lausanne, Switzerland

Edited by Joseph S. Takahashi, The University of Texas Southwestern Medical Center, Dallas, TX, and approved November 25, 2020 (received for review July 29, 2020)

The circadian clock and feeding rhythms are both important regulators of rhythmic gene expression in the liver. To further dissect the respective contributions of feeding and the clock, we analyzed differential rhythmicity of liver tissue samples across several conditions. We developed a statistical method tailored to compare rhythmic liver messenger RNA (mRNA) expression in mouse knockout models of multiple clock genes, as well as PARbZip output transcription factors (*Hlf*/*Dbp*/*Tef*). Mice were exposed to ad libitum or night-restricted feeding under regular light–dark cycles. During ad libitum feeding, genetic ablation of the core clock attenuated rhythmic-feeding patterns, which could be restored by the night-restricted feeding regimen. High-amplitude mRNA expression rhythms in wild-type livers were driven by the circadian clock, but rhythmic feeding also contributed to rhythmic gene expression, albeit with significantly lower amplitudes. We observed that *Bmal1* and *Cry1/2* knockouts differed in their residual rhythmic gene expression. Differences in mean expression levels between wild types and knockouts correlated with rhythmic gene expression in wild type. Surprisingly, in PARbZip knockout mice, the mean expression levels of PARbZip targets were more strongly impacted than their rhythms, potentially due to the rhythmic activity of the D-box–repressor NFIL3. Genes that lost rhythmicity in PARbZip knockouts were identified to be indirect targets. Our findings provide insights into the diurnal transcriptome in mouse liver as we identified the differential contributions of several core clock regulators. In addition, we gained more insights on the specific effects of the feeding–fasting cycle.

circadian clock | feeding–fasting cycle | liver metabolism | transcriptomics | differential rhythmicity analysis

Almost all organisms are subjected to daily changes in their environment with light–dark cycles that are caused by Earth's rotation around its own axis. To anticipate these changes, organisms possess an evolutionarily conserved endogenous oscillator, the circadian clock, that drives daily rhythms in behavior and physiology with a 24-h period (1, 2). In mammals, the circadian clock is hierarchically organized, with a master pacemaker located in the bilateral hypothalamic superchiasmatic nuclei (SCN) and peripheral clocks present in virtually all organs, including the liver (3, 4). The SCN clock receives light via the retina and transmits this information to the peripheral clocks via direct nervous connections or controlled secretion of humoral factors. On a molecular level, the circadian clock consists of interconnected transcriptional and translational negative-feedback loops of so-called clock genes (5). The core oscillator loop consists of a positive limb in which BMAL1 (named also ARNTL) and its heterodimerization partners CLOCK and NPAS2 promote gene expression of several clock target genes via E-box motifs. These include *Period* (*Per*) and *Cryptochrome* (*Cry*), factors of the negative limb of the core loop, which then in turn inhibit the transcriptional activity of BMAL1. In addition to this core loop, another crucial loop exists in which BMAL1 heterodimers target RORα, RORγ, REV-ERBα (also named NR1D1), and REV-ERBβ (also named NR1D2) regulate expression of *Bmal1* and its heterodimeric partners by binding to response elements (RORE) present in their promotors (6, 7). Furthermore, the circadian clock controls the expression of proline and acidic amino acid-rich basic leucine zipper (PARbZip) transcription factors DBP, HLF, and TEF and their repressive counterpart NFIL3 (named also E4BP4) factors. In vivo experiments in mice indicate that these transcription factors are not directly involved in the circadian clock machinery but

Significance

The rotation of the Earth around its own axis creates daily changes in the environment for virtually all living organisms. To anticipate and adapt to those changes, mammals possess an evolutionarily conserved circadian clock that controls most aspects of physiology. Using a previously undescribed analysis tool, we studied the impact of the circadian clock and its underlying feeding rhythms on hepatic gene expression. Our analysis shows that the loss of feeding rhythms in clock-disrupted animals is an important component of their phenotype. Finally, we were able to decipher the specific role of feeding rhythms, the circadian clock, and its controlled output of PARbZip transcription factors in the regulation of liver rhythmic gene expression.

Author contributions: B.D.W., C.G., F.N., and F.G. designed research; B.D.W., F.A., E.M., A.C., M.W., and F.G. performed research; B.D.W., C.G., F.P.A.D., N.E.P., and F.N. contributed new reagents/analytic tools; B.D.W., C.G., F.N., and F.G. analyzed data; B.D.W., M.W., and F.G. wrote the paper; B.D.W. designed the web application; and F.P.A.D. designed and implemented the web application.

Competing interest statement: B.D.W., C.G., F.A., E.M, A.C., and F.G. were employees of Société des Produits Nestlé SA.

This article is a PNAS Direct Submission.

[1]Present address: L'institut du thorax, Université de Nantes, FR-44007 Nantes, France.

[2]Present address: Swiss Integrative Center for Human Health, CH-1700 Fribourg, Switzerland.

[3]Present address: Sophia Genetics, CH-1202 Geneva, Switzerland.

[4]To whom correspondence may be addressed. Email: felix.naef@epfl.ch or f.gachon@uq.edu.au.

This article contains supporting information online at https://www.pnas.org/lookup/suppl/doi:10.1073/pnas.2015803118/-/DCSupplemental.

Published January 15, 2021.

mediate circadian clock output pathways via D-box elements (8, 9). To date, the relative contribution of each loop of the molecular network to rhythmic gene expression has been unclear.

In the liver, this oscillatory network regulates systems-wide rhythmic gene expression programs (10), including components of fundamental metabolic pathways (11). The cell-autonomous liver clock directly regulates genes involved in the regulation of glucose metabolism or xenobiotic detoxification through the positive loop and BMAL1 (12, 13). In addition, the PER and CRY proteins of the negative loop indirectly regulate lipid and glucose metabolism through interaction with nuclear receptors and cellular signaling (14–17). Nevertheless, the circadian clock is not the only driver of hepatic rhythmic gene expression. The SCN synchronize the peripheral clocks, including the liver clock, but also regulate systemic cues, such as locomotor activity, body temperature, and feeding and drinking behavior (18, 19). There is increasing evidence that daily food intake has a major impact on rhythmic gene expression and liver physiology. Specifically, feeding during the night, the activity phase of nocturnal animals like mice, increases the rhythmic amplitudes of liver physiology (20), while feeding during the resting phase inverts the temporal pattern of liver gene expression (21, 22). Constant feeding suppresses a large fraction of rhythmic gene expression in the liver (21, 23, 24). Nevertheless, the interplay of feeding cycles and the cell-autonomous clock on rhythmic gene expression in the liver is not fully understood.

A major reason for this gap of knowledge is the lack of comprehensive transcriptome datasets and analysis methods to investigate differential rhythmic gene expression in clock-disrupted mouse models and under varying feeding regimens. Here, we generated murine transcriptome datasets to systematically dissect the contribution of the molecular clock network and the role of natural feeding cycles on the temporal liver transcriptome. We performed transcriptome analyses of multiple circadian clock gene knockout (KO) models. This included the KO of the positive limb (*Bmal1* KO) or the negative limb (*Cry1/2* KO) of the core clock loop under ad libitum (AL) and night restricted-feeding (NRF) regimens. In addition, we assessed the role of the PARbZip-mediated clock output pathway using *Hlf/Dbp/Tef* KO mice. Moreover, we have implemented a statistical framework to assess differential rhythmicity and mean gene expression across multiple conditions. Our work defines the respective contributions of different components of the circadian clock network and of natural feeding cycles on rhythmic gene expression.

Results

A Statistical Framework to Detect Differential Rhythmicity across Many Conditions. While an increasing number of statistical methods allow the analysis of rhythmicity from time-series gene expression analysis, algorithms to assess differential rhythmicity across multiple conditions remain scarce (25, 26). Previously, we have used harmonic regression and model selection to assess differential rhythmicity between conditions in various settings (27–33). The key idea is that rhythmicity parameters (amplitude and phase) for each condition can be shared across subsets of conditions, leading to a combinatorial set of possible models for each gene (*SI Appendix*, Fig. S1 *A* and *B*). By assigning each gene (probabilistically) to one of these models (Fig. 1*A*), this method provides a powerful alternative to common approaches based on intersecting the identified sets from the individual conditions, which is typically sensitive to thresholds. However, the method had to be customized for each specific setting and was not implemented into a flexible and accessible statistical package. We have now extended this method to detect and estimate changes in the parameters amplitude ($\log_2$ fold-change peak-to-trough), phase (time of peak), and mean expression levels for datasets with two or more conditions. Moreover, the models are now tailored to the noise properties of RNA-sequencing (RNA-Seq) data. The method was named *dryR* (for Differential Rhythmicity Analysis in R) and is available as an R package (https://github.com/naef-lab/dryR).

To systematically assess the performance of *dryR* and compare it with existing rhythmicity analysis methods, we simulated rhythmic count data for four conditions with a commonly used sampling interval of 4 h and two replicates. We first tested goodness of fit of *dryR* and detected overall good fits for phase, mean, and amplitude with higher noise at lower mean counts (*SI Appendix*, Fig. S1*C*). In a second step, we used simulations to test the reliability of detecting rhythmicity in four conditions and benchmarked it to published rhythm-detection methods (*SI Appendix*, Fig. S1*D*). The number of correctly detected rhythms across all four conditions was in the same range as with best-performing other algorithms, for which each condition was tested individually. Moreover, *dryR* performed reliably across a broad spectrum of conditions, including varying sampling intervals, missing samples, and numbers of replicates (*SI Appendix*, Fig. S1*E*). Next, we compared the ability of *dryR* to detect phase shifts and changes in amplitude with methods designed for differential rhythmicity analysis between two conditions of temporal data: CircaCompare (34), Detection of Differential Rhythmicity (35), and LimoRhyde (36). To this end, we simulated rhythmic data with either a 4-h phase shift or a doubling in amplitude between two conditions. *dryR* reliably performs the calling of differential rhythmicity with comparable specificity and sensitivity as the best-performing algorithms across variable sampling intervals or changing numbers of replicates and missing samples (*SI Appendix*, Fig. S1 *F–I*). Thus, the performance of *dryR* is comparable to other methods for detecting rhythmicity or differential rhythmicity, but the advantage of *dryR* is that it combines rhythmicity detection, differential gene expression, and rhythmicity analysis for two or more conditions.

Clock-Disrupted Mice Exhibit Attenuated Feeding Rhythms, Dampening Rhythmic Liver Gene Expression. The fasting–feeding cycle is an important driver of rhythmic gene expression in the mouse liver (21, 23, 24). To distinguish the contribution of natural feeding cycles (food intake occurs largely during the night in wild-type [WT] animals with free access to food [AL]), and of the circadian clock to rhythmic gene expression, we kept *Cry1/2* and *Bmal1* KO mice and WT controls under a 12-h light–dark cycle under AL feeding (Fig. 1*B*). Compared with WT animals, both *Bmal1* and *Cry1/2* KOs lost their feeding rhythms under AL feeding (Fig. 1C). In parallel, to control for feeding rhythms, we conducted the same experiment with restricted access to food during the active phase (NRF) (Fig. 1*B*). As expected, feeding rhythms comparable to WT AL were found in the KOs under NRF (Fig. 1*C*).

We then investigated temporal gene expression in the liver of these mice using RNA-Seq (sampled every 4 h, two independent replicates) and analyzed the results by *dryR*. The vast majority of circadian core clock genes lost rhythmicity in *Bmal1* and *Cry1/2* KOs irrespective of the offered feeding regimen (*SI Appendix*, Figs. S2*A* and S3 and Dataset S1), except for *Per2*, consistent with previous work (37). Moreover, of all transcripts assigned to a model with identical rhythms in WT AL and NRF (Fig. 1 *D* and *E*), a comparable proportion was detected to be regulated by the circadian clock (clock-driven) in both *Bmal1* KO (30%; Fig. 1*D*) and *Cry1/2* KO (37%; Fig. 1*E*). Accordingly, these transcripts lost rhythmicity in both KO AL and KO NRF. We next used the KO mice under both feeding regimens to identify transcript rhythms that depend on a natural feeding–fasting cycle. In WT animals, AL and NRF showed similar numbers of cyclic genes across the entire range of amplitudes, with nearly 100 transcripts with amplitudes above 8-fold in both genotypes (Fig. 1*F*). In contrast, at least 32% and 54% of rhythmic transcripts under NRF

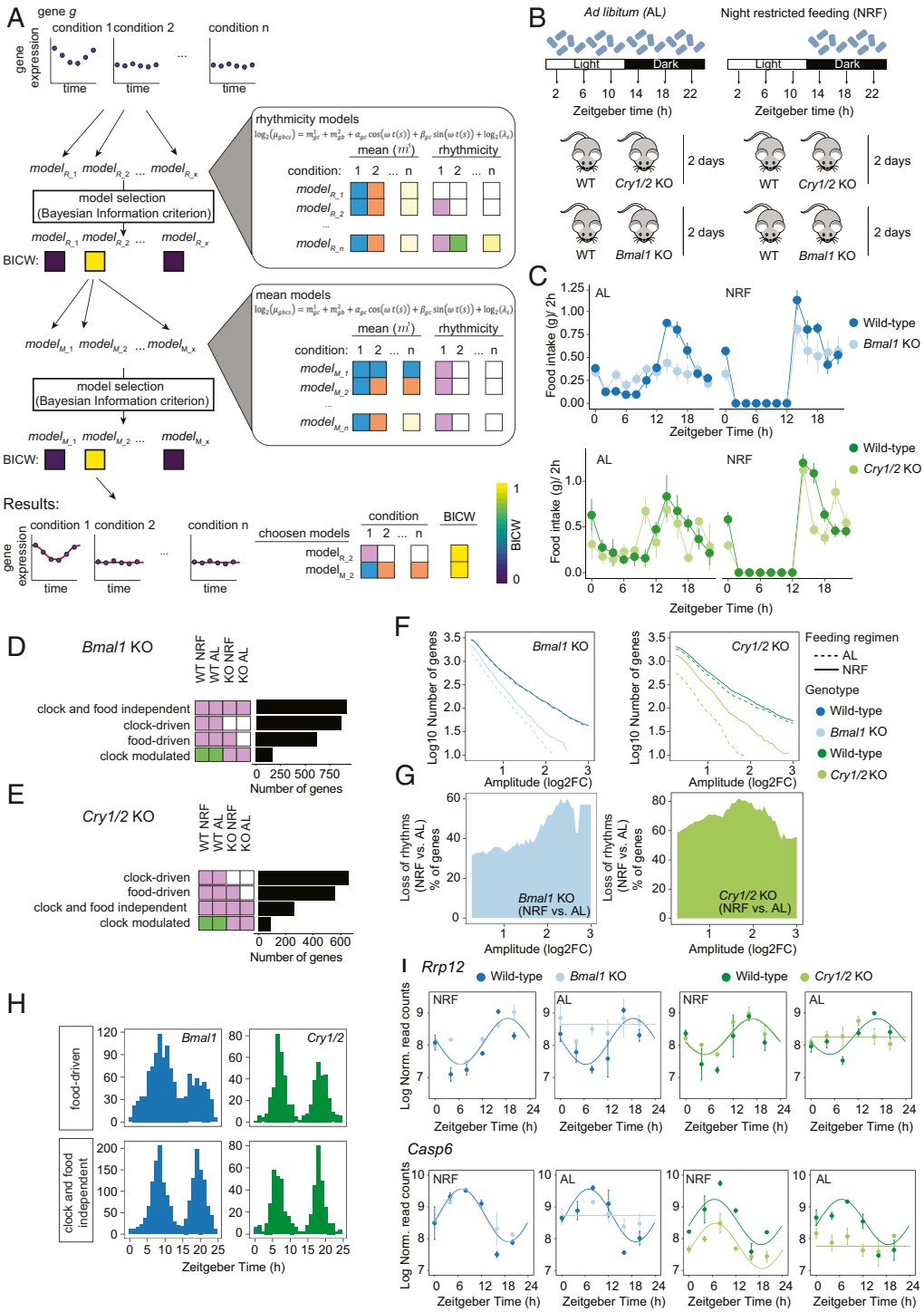

Fig. 1. Regulation of liver rhythmic gene expression by the circadian clock and feeding rhythms analyzed with *dryR*. (*A*) Schematic illustrating the workflow of the statistical framework used in *dryR*. BICW is color-coded as indicated in the ramp (*Lower Right*). The same color for the remaining boxes indicates shared mean levels and rhythmic parameters between the indicated conditions for mean and rhythmic models, respectively. (*B*) Experimental design. (*C*) Rhythmic feeding in WT, *Bmal1* KO, and *Cry1/2* KO mice under AL and NRF. The Zeitgeber time (ZT) defines the timing of entrainment by light (ZT0 lights on; ZT12: lights off). (*D* and *E*) Number of genes classified in rhythmic models in *Bmal1* KO (*D*) and *Cry1/2* KO (*E*). White indicates no rhythm detected, and the same color indicates shared rhythmic parameters (amplitudes and phase) between the indicated conditions. (*F*) Cumulative number of rhythmic genes in the liver of WT, *Bmal1* KO, and *Cry1/2* KO in function of minimal amplitude. NRF partially restores rhythmicity in KOs. (*G*) Relative number of genes that lose rhythmicity under the AL compared with NRF regimen in KO in function of minimal amplitude. (*H*) Phase distribution of rhythmic genes classified as food-driven and clock- and food-independent. (*I*) Temporal expression pattern of *Rrp12* and *Casp6*.

lost rhythmicity in the absence of rhythmic food intake (AL) in *Bmal1* and *Cry1/2* KOs, respectively, across the entire range of amplitude (Fig. 1 *F* and *G*). Among those, transcripts assigned to the food-driven model comprised 22% (*Bmal1* KO; Fig. 1*D*) and 31% (*Cry1/2* KO; Fig. 1*E*) of all rhythmic genes. These transcripts shared amplitude and phase across three conditions

(WT AL, WT NRF, and KO NRF) but lost rhythmic expression in the absence of rhythmic food intake (KO AL) (Fig. 1 *D* and *E* and *SI Appendix*, Fig. S2*B*). These feeding–fasting-driven rhythmic genes (food-driven) exhibited a bimodal phase distribution (Fig. 1*H* and *SI Appendix*, Fig. S2*C*) and on average 36% lower amplitudes (*SI Appendix*, Fig. S2*D*) compared with clock-driven or clock-modulated genes. As exemplified by *Rrp12* (night phase) and *Casp6* (light phase) (Fig. 1*I*), they lost rhythmicity in the KOs under AL feeding, while they retained rhythms under NRF conditions. Of all rhythmic genes, 5% (*Bmal1* KO) and 6% (*Cry1/2* KO) were regulated by feeding rhythms but showed different rhythmic parameters (i.e., amplitude and/or phase) in the KO, suggesting that feeding rhythms and the clock participate in their regulation (clock-modulated; Fig. 1 *D* and *E* and *SI Appendix*, Fig. S2*B*). Strikingly, 32% (*Bmal1* KO) and 14% (*Cry1/2* KO) of rhythmic genes exhibited consistent rhythmicity (identical phases and amplitudes) across all four tested conditions (clock- and food-independent; Fig. 1 *D* and *E* and *SI Appendix*, Fig. S2 *B–D*). Clock- and food-independent rhythms also exhibited a biphasic phase pattern (Fig. 1*H*) and showed amplitudes comparable to (*Bmal1* KO) or lower (*Cry1/2* KO) than those of food-driven transcripts (*SI Appendix*, Fig. S2 *B–D*). For example, *Cirbp* and *Hsp90ab1* keep rhythmic messenger RNA (mRNA) levels in all conditions (*SI Appendix*, Fig. S2*E*). These findings suggest that under a light–dark cycle, additional clock-independent systemic signals other than feeding drive low-amplitude rhythmic gene expression in the liver.

Clock- and System-Driven Biological Functions of the Rhythmic Liver Transcriptome. To further distinguish the specific contribution of the core clock oscillator from rhythmic feeding on rhythmic gene expression in the mouse liver, we focused our analysis on *Bmal1* and *Cry1/2* KO animals kept under NRF. Using *dryR*, genes were grouped according to their temporal expression patterns into five categories (system-driven, clock-driven, clock-modulated, *Cry1/2* KO-specific, *Bmal1* KO-specific) (Fig. 2 *A* and *B* and Dataset S2). Of all rhythmic genes in WT mice, 33% were independent of a functional clock and remained rhythmic in both KOs and, thus, were named system-driven. Expectedly, these gene promoters lacked binding of circadian clock transcription factors (*SI Appendix*, Fig. S4*A*). System-driven genes turned out to exhibit lower amplitudes compared with clock-driven or clock-modulated genes (Fig. 2*C* and *SI Appendix*, Fig. S4 *B* and *C*) and showed a bimodal phase distribution (Fig. 2*D* and *SI Appendix*, Fig. S4*B*). In a temporal resolved-enrichment analysis, these system-driven genes can be assigned to mRNA translation and ribosome biogenesis ("ribosome biogenesis," "nucleolus," and "de novo posttranslational folding"), known to be regulated by systemic signals (32), and metabolism of food ("cellular lipid metabolic process" and "response to insulin") (Fig. 2*E*). Moreover, immune function ("BCR B-cell") was also enriched for system-driven genes, which is likely a consequence of the rhythmic circulation of B cells (38). In comparison, clock-driven genes, which lost rhythmicity in the KO mice, represented 20% of all rhythmic genes in the mouse liver (Fig. 2*A*). These genes had generally a high amplitude (Fig. 2*C* and *SI Appendix*, Fig. S4 *B* and *C*). Interestingly, this gene set showed a homogenous distribution of peak times (Fig. 2*D* and *SI Appendix*, Fig. S4*B*). Clock-driven genes could be assigned, besides their evident role in the circadian clock oscillator, to a function in metabolism of xenobiotics ("xenobiotic metabolism" and "biotransformation"), a process previously implicated with the circadian clock (39). Surprisingly, we also found a hitherto unknown clock-driven function in ion transport ("Na^{2+} transmembrane transporter activity") (Fig. 2*E*). Like the clock-driven genes, the set of clock-modulated genes was targeted by the circadian core clock factors but displayed an altered rhythmic oscillation in the absence of a functional clock (7%; Fig. 2*A* and *SI Appendix*, Fig. S4*A*). These genes shifted from a pattern resembling clock-driven genes that show a homogeneous phase distribution, to a bimodal phase distribution in clock-disrupted animals with lower amplitude, a pattern similar to what was observed for system-driven genes (Fig. 2*D* and *SI Appendix*, Fig. S4 *B* and *D*). Clock-modulated genes appeared to play a role for the immune system and interferon response ("IRF target genes"), known as a rhythmic process (40) and the modulation of food-related insulin response ("insulin signalling") (Fig. 2*E*). Together, our observations suggest that systemic signals generate bimodal and low-amplitude rhythmicity in gene expression in the mouse liver, whereas the circadian clock drives gene expression rhythms with high amplitudes covering all phases.

Differential Rhythmicity between *Bmal1* and *Cry1/2* KO Models in Liver Gene Expression. The transcriptional circuitry of the mouse circadian clock is a complex network of positive- and negative-feedback loops. Our dataset containing KOs for *Bmal1* and *Cry1/2* allows the comparison of the effects of the core transcriptional activator BMAL1 and its repressors CRY1 and CRY2. Therefore, we continued to characterize the differential effects on rhythmic liver gene expression in these KOs under NRF in 12-h light–dark cycles. We detected genes that lost rhythmicity only in one of the KOs (i.e., rhythms that were lost in either *Bmal1* KO or *Cry1/2* KO; Fig. 2 *A–D*). The amplitudes of these rhythmic transcript were overall lower than clock-driven and comparable to system-driven transcripts (*SI Appendix*, Fig. S4*C*). These findings suggest that systemic signals blunted specifically in *Bmal1* or *Cry1/2* KO can modulate rhythmic gene expression. Indeed, glucocorticoid responsive genes ("Prednisolone induced" and "Glucocorticoid dependent rhythmic genes") are more likely to lose rhythm specifically in *Cry1/2* KO (Fig. 2*E*), which might reflect the direct repression of the glucocorticoid receptor by CRY1 and CRY2 (16). Conversely, loss of rhythms related to mitochondrial activity and metabolism of glycolipids were more specific to the deletion of *Bmal1* (Fig. 2*E*).

We further analyzed genes showing a phase shift in the two KO models. Interestingly, in *Cry1/2* KO mice under NRF, a subset of rhythmic genes exhibited a phase advance of ∼4 h compared with WT (*SI Appendix*, Fig. S5*A*). In comparison, *Bmal1* KO mice did not show such biased phases (*SI Appendix*, Fig. S5*A*). To identify potential transcription factors involved in this phase shift, we performed an untargeted ChIP-enrichment analysis (Dataset S2). This revealed that CREB- and PPARα-binding sites are significantly enriched in genes with a phase differences in the two KO models. While CREB activity has been shown to be phase-delayed in *Bmal1* KO mice (41), PPARα potentially mediates the phase advance in *Cry1/2* KO mice. Indeed, PPARα target genes were enriched not only in clock-driven genes but also in genes showing altered rhythms in both KOs (*SI Appendix*, Fig. S5*B*). Moreover, only in *Cry1/2* KO, PPARα target genes showed a phase advanced of 4 h (*SI Appendix*, Fig. S5*A*), as exemplified by *Pnpla2*, *Lpin2*, and *Cpt1a* (*SI Appendix*, Fig. S5*C*). While expression of *Pparα* was slightly decreased in *Bmal1* KO, as previously shown (42), we did not detect any rhythmicity changes of *Pparα* mRNA expression in *Cry1/2* KO (*SI Appendix*, Fig. S5*D*). However, nuclear PPARα protein levels were phase-advanced (*SI Appendix*, Fig. S5*E*) based on published nuclear proteomics data (43). Together, the *Bmal1* and *Cry1/2* KOs show both shared effects on clock-driven genes expression as well as distinct differences in rhythmic gene expression in the liver.

Changes in Mean mRNA Levels in *Bmal1* and *Cry1/2* KOs Predict Amplitude and Distinct Expression Phases. Most circadian transcriptome studies across several conditions (altered feeding,

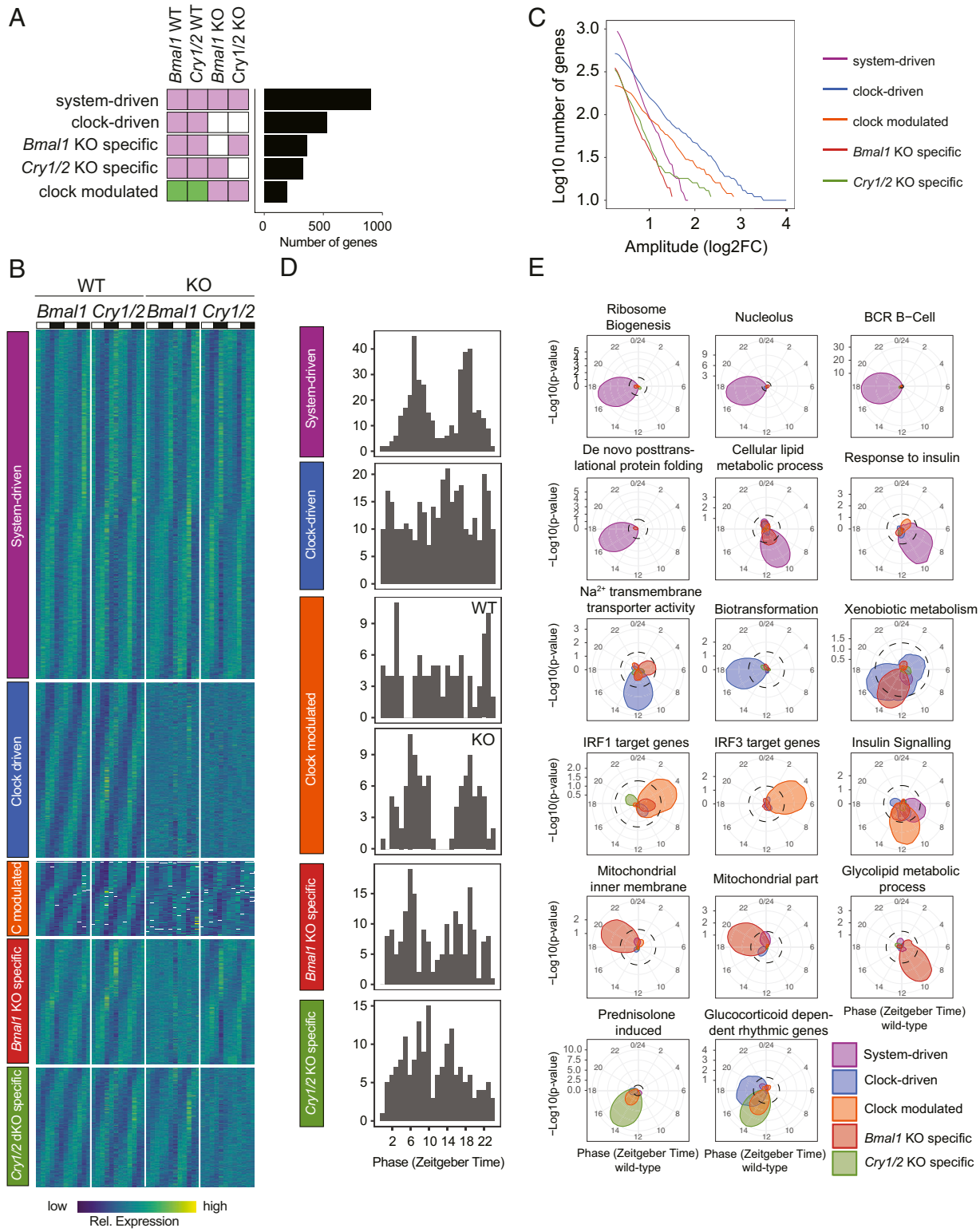

Fig. 2. Systemic cues and the circadian clock equally shape rhythmic liver gene expression. (*A*) Number of genes classified in rhythmic models in *Bmal1* KO and *Cry1/2* KO under NRF. White indicates no rhythm detected, and the same color indicates shared rhythmic parameters (amplitudes and phase) between samples. (*B*) Heat maps of normalized rhythmic mRNA levels in the liver of WT, *Bmal1* KO, and *Cry1/2* KO mice. Genes were classified as system-driven, clock-driven, *Bmal1* KO-specific, *Cry1/2* KO-specific, and clock-modulated. (*C*) Cumulative number of genes classified in the indicated rhythmic model in function of minimal amplitude. (*D*) Phase distribution of indicated models. (*E*) Examples of functional enrichment around the clock. Enrichment of the indicated functional terms is represented by the radial coordinate at the indicated time point. *P* values were calculated by comparing the genes within a sliding window of 4 h with all expressed genes.

KOs) have focused on rhythmic gene expression but have not investigated changes in mean mRNA levels. Therefore, we used the *dryR* framework to detect patterns in mean mRNA levels (Fig. 1*A*) and learn about circadian clock-regulated gene expression. Overall, more genes were differentially expressed in *Bmal1* KO than in *Cry1/2* KO mice (Fig. 3*A*). Consistent with the molecular function of BMAL1 as a positive regulator of transcription and CRY1/2 as a repressor in the core clock loop, more genes were down-regulated (compared with up-regulated) in *Bmal1* KO and vice versa in *Cry1/2* KO mice (Fig. 3*B*), indicating that the direct effects of those transcription regulators are dominant.

Next, we elucidated the relationships between changes in mean levels in the KOs and rhythmicity in liver gene expression. Genes that shared their mean expression across all four conditions were more likely nonrhythmic. Conversely, genes that showed differential mean levels between KO and WT were enriched among clock-driven and clock-modulated rhythmic genes (Fig. 3*C*). We next compared mean gene expression changes in both KOs and grouped genes accordingly (Fig. 3*D*). Target genes of E-box– or D-box–binding core clock and clock output proteins (i.e., BMAL1, CLOCK, NPAS2, CRY1/2, PER1/2, DBP, and NFIL3) were down-regulated in *Bmal1* KO mice and derepressed in *Cry1/2* KOs (Fig. 3 *D* and *E*). On the other hand, genes regulated by the BMAL1-regulated repressors NR1D1 and NR1D2 showed opposite mean differences (Fig. 3 *D* and *E*). Interestingly, among core clock and clock-related genes, only *Npas2* and *Rorγ* showed atypical patterns. *Npas2* was the only clock gene that showed a clear up-regulation in expression in *Cry1/2* KO and a down-regulation in *Bmal1* KO (Fig. 3*D* and *SI Appendix*, Fig. S3), further supporting the idea that *Npas2* is a NR1D1/2 and ROR target (44). Surprisingly, the mean levels of *Rorγ* were up-regulated in both KOs (Fig. 3*D* and *SI Appendix*, Fig. S3). Our observation points to a complex feedback regulation in the circadian oscillatory core loop, as supported by others (45). The reported regulation of *Rorγ* by both NR1D1/2 and BMAL1 might play a role in this complex regulation (46).

Finally, we established how quantitative differences in mean level between KO and WT correlated with rhythmic parameters such as phase and amplitude. To this end, we calculated a double-difference score (ΔΔ*Bmal1*/*Cry1/2*) summarizing the effects of changes in both *Cry1/2* KO and *Bmal1* KO (Fig. 3*F*). The absolute ΔΔ*Bmal1*/*Cry1/2* value correlated with amplitude, while genes expressed at different phases showed a bias in positive or negative values (Fig. 3*G*). For example, genes expressed near ZT14 showed predominantly negative values. Conversely, the phase distributions differed depending on the ΔΔ*Bmal1*/*Cry1/2*. Indeed mRNA levels of genes with a negative ΔΔ*Bmal1*/*Cry1/2* (e.g., *Usp2*) were peaking around ZT14 (Fig. 3 *G*–*I*), fitting to the reported activity (9, 47) and nuclear protein levels of E-box and D-box transcriptional factors (43). Genes with a positive ΔΔ*Bmal1*/*Cry1/2* (e.g., *Loxl4*) exhibited phases reminiscent of RORα/γ and NR1D1/2 target genes (Fig. 3 *G*–*I*). Overall, opposing transcriptional changes in *Bmal1* KO and *Cry1/2* KO correlate with rhythmicity, higher amplitudes, and preferred peak phases.

PARbZip Target Genes Remain Rhythmic with Lower Mean Expression in the Liver of *Hlf*/*Dbp*/*Tef* KO Mice. To interfere with further regulators of rhythmic gene expression, we extended our analysis to D-box transcriptional regulators (HLF, DBP, and TEF) that mediate outputs of the circadian clock (39, 48). To this end, *Hlf*/*Dbp*/*Tef* KO and WT mice were exposed to a light–dark cycle under an AL feeding regimen (Fig. 4*A*). *Hlf*/*Dbp*/*Tef* KOs exhibited an intact circadian locomotor activity, as previously shown (48), and conserved feeding rhythms comparable to those in WT under AL (Fig. 4*B*), unlike the core clock KO animals (Fig. 1*C*). Liver transcriptome analysis using *dryR* (sampled every 4 h, two independent replicates) showed that the lack of the circadian clock output regulators HLF, DBP, and TEF had little effect on the rhythmic expression patterns of circadian clock genes and showed only minor effects on the mean expression level of a few circadian clock genes (*SI Appendix*, Fig. S6 *A* and *B* and Dataset S3). Overall, the number of rhythmic transcripts in *Hlf*/*Dbp*/*Tef* KOs was 18% lower than in WT mice, uniformly across the entire range of amplitudes (Fig. 4*C* and *SI Appendix*, Fig. S6*C*). Specifically, amplitude and phase of most oscillating genes in WT (59%) were unaltered in *Hlf*/*Dbp*/*Tef* KOs while 28% of rhythmic genes lost rhythmicity in the KO and depended on the presence of PARbZip regulators (Fig. 4 *D* and *E* and *SI Appendix*, Fig. S6*D*); 10% of all rhythmic genes were oscillating only in *Hlf*/*Dbp*/*Tef* KOs (Fig. 4 *D* and *E* and *SI Appendix*, Fig. S6*D*). Unaltered rhythmic genes were not only genes showing promoter-bound E-box and RORE transcriptional regulators but unexpectedly also by D-box transcriptional regulators such as DBP and NFIL3 (Fig. 4*F*). Conversely, rhythmic genes that lost rhythms in PARbZip-deficient mice were not enriched in direct targets of D-box transcriptional regulators (Fig. 4*F*), hinting at indirect effects.

We next used *dryR* to assess differential mean level changes in the *Hlf*/*Dbp*/*Tef* KOs (*SI Appendix*, Fig. S6 *E* and *F*). Genes with a loss of rhythm, but surprisingly also those with an unaltered rhythm, were more often down-regulated than up-regulated in *Hlf*/*Dbp*/*Tef* KOs (Fig. 4*G*). Many of the strongly down-regulated rhythmic genes exhibited a peak in phase at ZT20, the phase typically shown by PARbZip target genes, whereas strongly up-regulated genes rather peaked in the opposite phase (Fig. 4 *H* and *I*).

We next checked which biological functions were overrepresented in the rhythmic mRNAs with altered mean expression level in *Hlf*/*Dbp*/*Tef* KOs. Major parts of the xenobiotic metabolic network were down-regulated but kept their rhythmic gene expression in *Hlf*/*Dbp*/*Tef* KOs (Fig. 4*J* and *SI Appendix*, Fig. S7 *A* and *B*). Some bona fide direct PARbZip target genes associated with xenobiotic metabolism (e.g., *Alas*, *Por*, *Car* [*Nr1i3*]) were down-regulated but maintained their rhythmic expression patterns in the KO (*SI Appendix*, Fig. S7*A*). Moreover, targets of the xenobiotic nuclear receptor CAR (NR1I3) also showed a similar expression pattern (e.g., *Ces1d*, *Cyp2b10*, *Akl4*) (*SI Appendix*, Fig. S7*A*). The second xenobiotic receptor PXR (NR1I2) and its target genes tended to keep rhythmic expression patterns in *Hlf*/*Dbp*/*Tef* KOs as well but showed a decreased expression level (*SI Appendix*, Fig. S7 *A* and *B*). The bile acid receptor FXR (NR1H4) is the only nuclear receptor that showed a robust loss of rhythms in *Hlf*/*Dbp*/*Tef* KOs and so did members of its target cascade, including *Nr0b2* (*Shp*) and *Cyp7a1* (*SI Appendix*, Fig. S7*A*), consistent with published results (49).

On the other hand, genes that lost rhythms in *Hlf*/*Dbp*/*Tef* KOs were associated with oxidative phosphorylation and ribosomes (Fig. 4*J* and *SI Appendix*, Fig. S7 *C* and *D*). Rhythmic levels of ribosome-associated genes have been linked to diurnal fluctuations of liver mass (50). We therefore tested whether a loss of liver size fluctuation in *Hlf*/*Dbp*/*Tef* KOs is associated with blunted rhythms in ribosome-associated genes. Indeed, *Hlf*/*Dbp*/*Tef* KOs lacked daily fluctuations and showed an overall larger liver mass (*SI Appendix*, Fig. S7*E*), potentially indicating that the two processes are interdependent. In conclusion, our studies revealed that disrupted PARbZip function resulted in a down-regulation of gene expression rather than a loss of rhythm of target genes. The observed loss of rhythms for some biological functions in the KO might be elicited by indirect effects such as a lack of liver size fluctuation.

NFIL3 and PARbZip Transcription Factors Cooperate to Drive Rhythmic Gene Expression in Liver. The D-Box–binding repressor NFIL3 (named also E4BP4) binds the same D-box motifs (51), and its mRNA was still rhythmically expressed in *Hlf*/*Dbp*/*Tef* KO mice

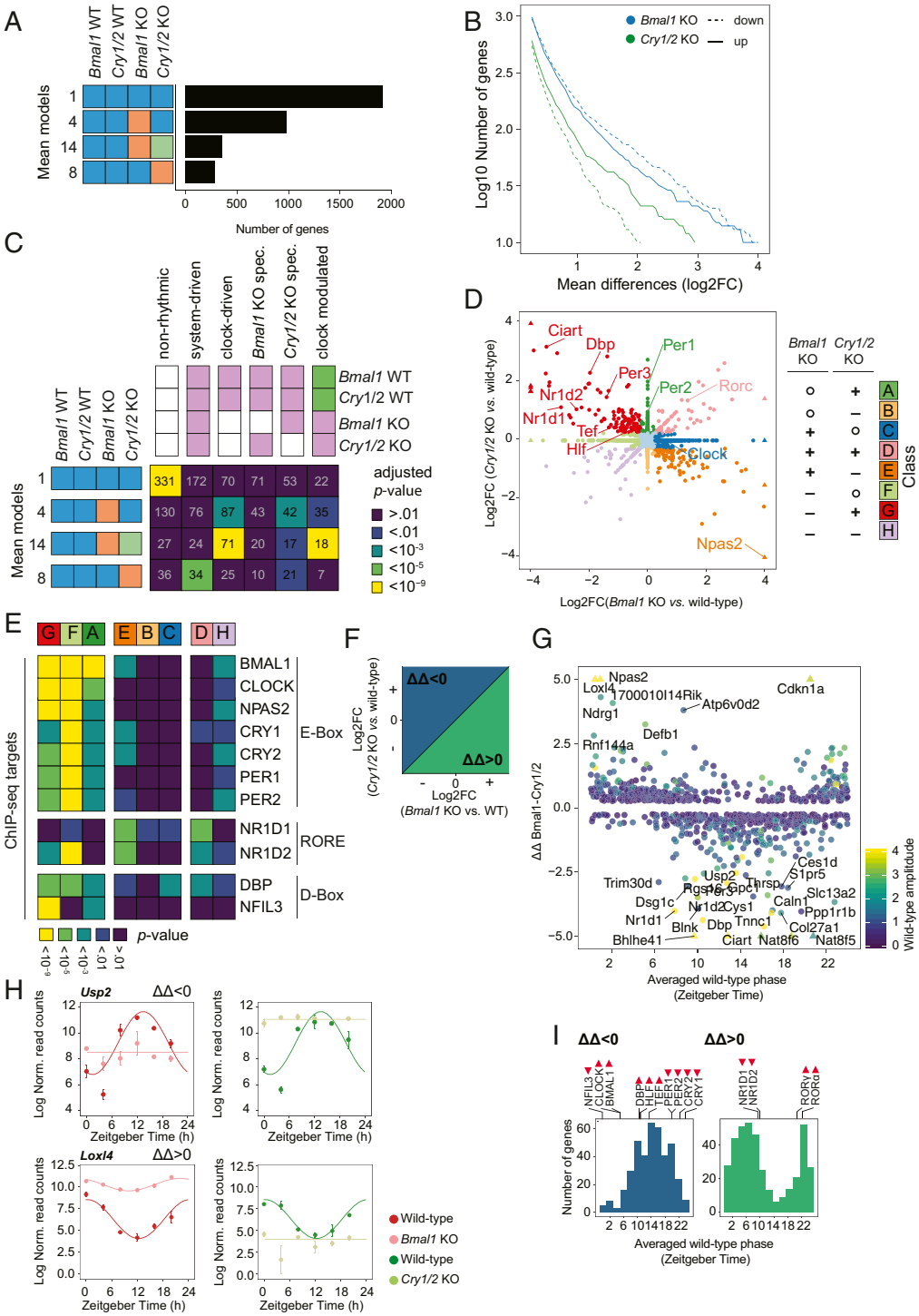

Fig. 3. Differential mean expression between KOs of the positive and negative limb can predict rhythmic parameters of gene expression. (*A*) Number of genes classified in mean models under NRF in *Bmal1* KO and *Cry1/2* KO. The same color indicates shared mean expression levels between samples. (*B*) Cumulative number of genes that are up-regulated and down-regulated in mean expression with a $\log_2$ fold-change larger than the value on the *x* axis between the indicated KO and WT. (*C*) Number of genes corresponding to the indicated mean and rhythm model. Genes that show constant mean expression levels in both KO models are more likely to display no rhythmicity. Genes with differences in mean levels in *Bmal1* KO or *Cry1/2* KO are more likely to also be rhythmically expressed. (*D*) Scatterplot of $\log_2$ fold-changes in mean levels in *Bmal1* KO vs. *Cry1/2* KO. The color represents classes that group genes according to their differential expression pattern in the two KOs (+, up-regulation; –, down-regulation; o, not differentially expressed). (*E*) Enrichment analysis of clock gene targets for differentially expressed genes in the indicated class. (*F*) Schematic of $\log_2$ fold-changes in mean levels in *Bmal1* KO/WT vs. *Cry1/2* KO/WT to indicate the meaning of a positive or negative $\Delta\Delta$*Bmal1*/*Cry1/2* ($\Delta\Delta$). (*G*) Scatterplot of phase in WT mice in function of the difference of $\log_2$ fold-changes in mean levels of *Bmal1* KO vs. WT and $\log_2$ fold-changes in mean levels of *Cry1/2* KO vs. WT ($\Delta\Delta$*Bmal1*/*Cry1/2*). (*H*) Example of rhythmic genes expression patterns with differing mean levels. (*I*) Phase histogram of genes with a positive or negative $\Delta\Delta$*Bmal1*/*Cry1/2*. Time of peak (▲) or trough (▼) of clock protein levels in liver nuclei (43) are indicated as triangles above the histograms.

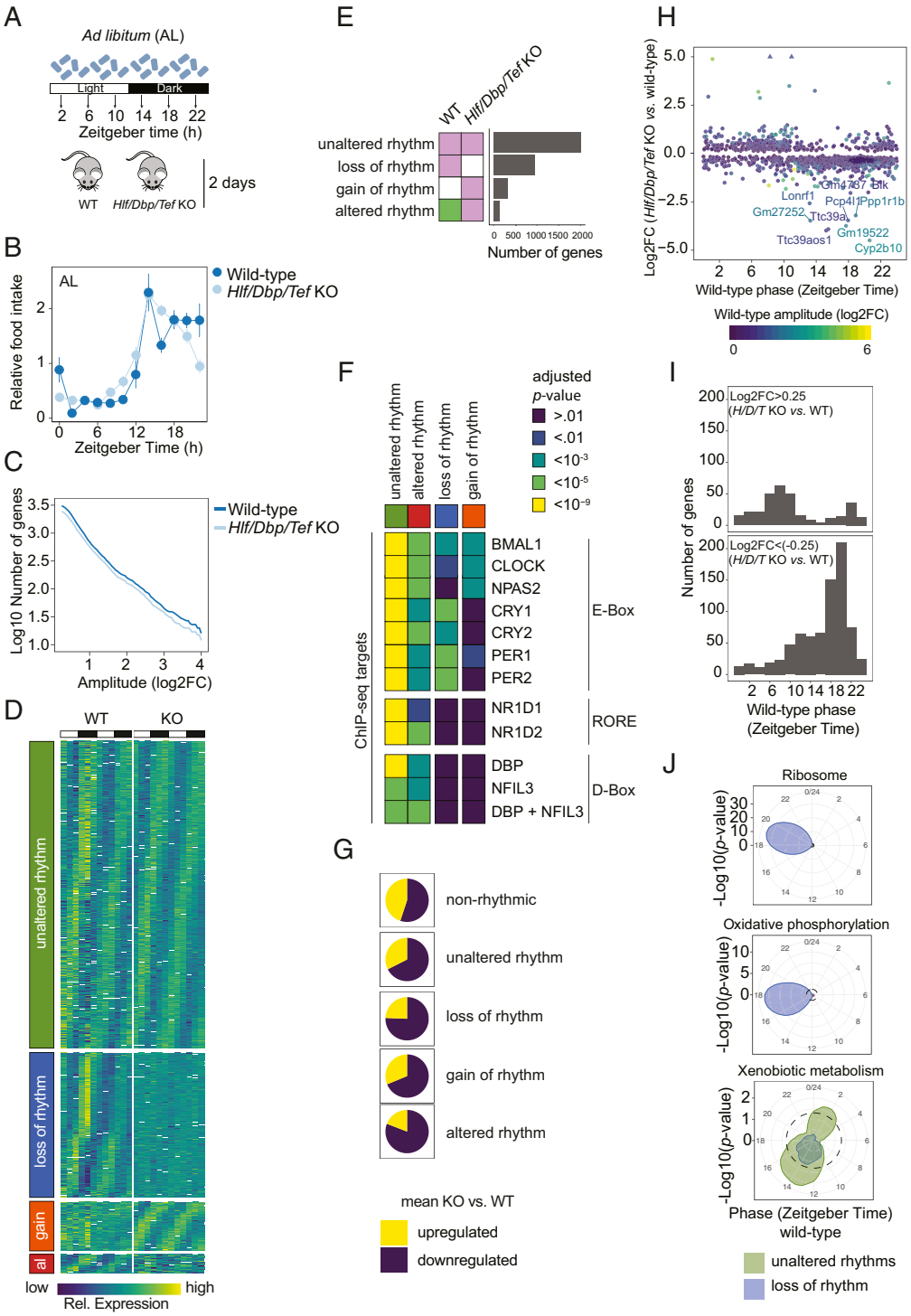

Fig. 4. PARbZip target genes have reduced expression in KO animals but maintain rhythmicity. (*A*) Experimental design. (*B*) Rhythmic-feeding patterns in WT and *Hlf/Dbp/Tef* KO mice under an AL feeding regimen. (*C*) Cumulative number of genes classified in the indicated rhythmic model in function of minimal amplitude. (*D*) Heat maps of normalized rhythmic mRNA levels in the liver of WT and *Hlf/Dbp/Tef* KO mice. Genes were classified according to their temporal expression pattern in *Hlf/Dbp/Tef* KO compared with WT mice: unaltered rhythm, loss of rhythm, gain of rhythm (gain), and altered rhythm (al). (*E*) Number of genes classified in models according to their hepatic temporal gene expression pattern in *Hlf/Dbp/Tef* KO and WT mice. White indicates no rhythm detected, and the same color indicates shared rhythmic parameters (i.e., amplitudes and phase) between the indicated conditions. (*F*) Enrichment analysis of clock gene targets for differentially expressed genes in the indicated class (for details, see *D*). (*G*) Ratio of mean differential gene expression in the liver of the indicated rhythm model. (*H*) Scatterplot of phase in WT mice in function of $\log_2$ fold-changes in mean levels in *Hlf/Dbp/Tef* KO vs. WT mice. (*I*) Phase distribution of genes that are up-regulated (*Top*) or down-regulated (*Bottom*) in their mean expression in *Hlf/Dbp/Tef* KO compared with WT mice. (*J*) Enrichment of the indicated functional terms is represented by the radial coordinate at the indicated time point. *P* values were calculated by comparing the genes within a sliding window of 4 h with all expressed genes.

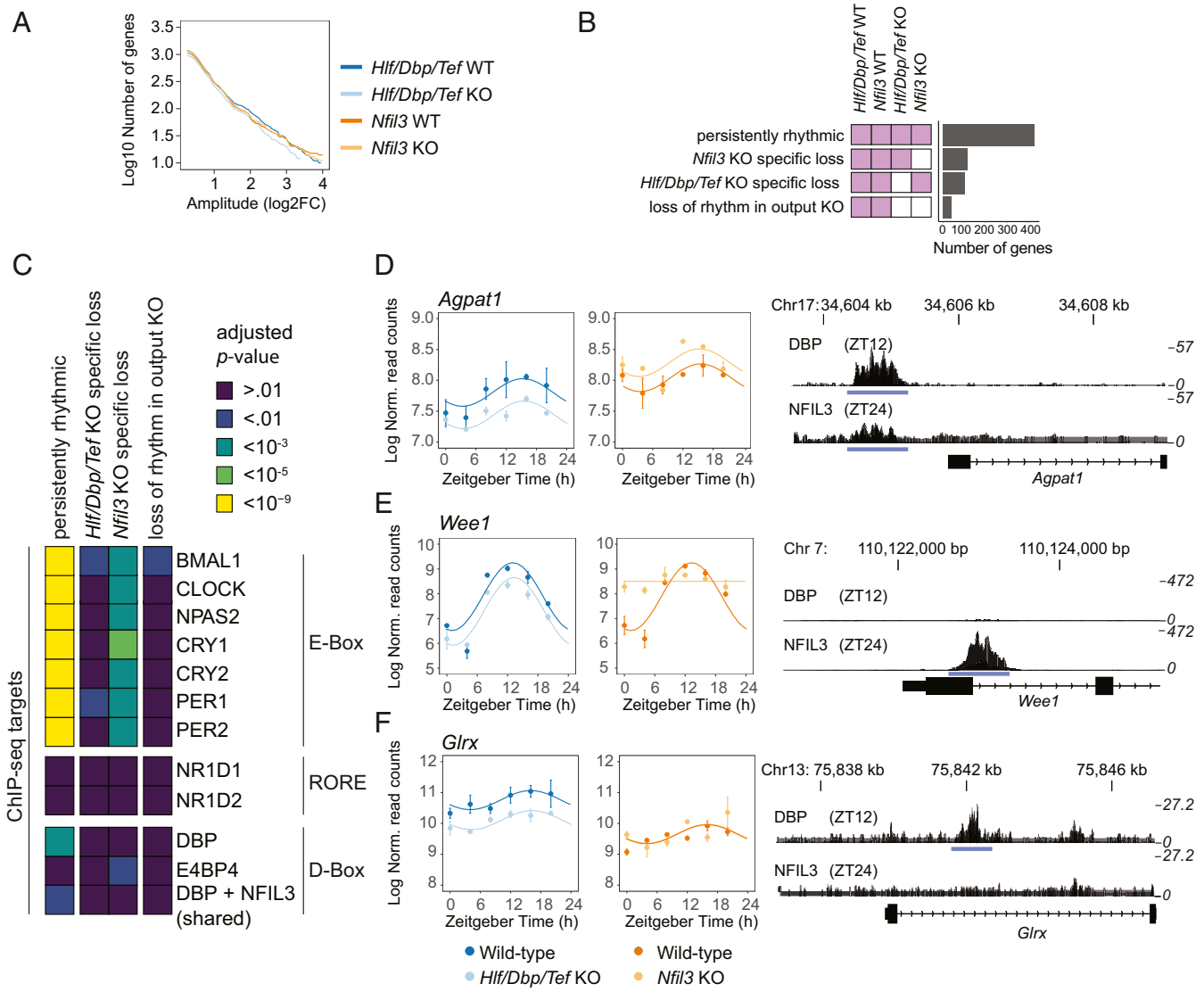

Fig. 5. Comparative analysis of differential liver expression in *Hlf/Tef/Dbp* KO and *Nfil3* KO mice. (*A*) Cumulative number of rhythmic genes with amplitudes larger than the value on the *x* axis in the indicated genotype. (*B*) Number of genes classified in models according to their liver gene expression profile in *Hlf/Dbp/Tef* WT, *Nfil3* WT, *Hlf/Dbp/Tef* KO, and *Nifl3* KO mice. White indicates no rhythm detected, and the same color indicates shared rhythmic parameters (i.e., amplitudes and phase) between indicated conditions. (*C*) Enrichment analysis of core clock targets for genes classified into the indicated rhythmic model. Target genes have been identified using published ChIP-Seq data in mouse liver (see *SI Appendix, SI Materials and Methods* for details). (*D–F*) Gene expression over time (*Left*) and ChIP-Seq profiles of DBP and NFIL3 at the promotor region of *Agpat1* (*D*), *Wee1* (*E*), and *Glrx* (*F*) (*Right*) in mouse liver. ChIP-Seq profiles are derived from published datasets in mouse liver (9).

(*SI Appendix*, Fig. S6*A*). Thus, NFIL3 potentially drives the remaining rhythmicity of PARbZip target genes in the liver of *Hlf*/*Dbp*/*Tef* KO mice. To test this assumption, we made use of a publicly available RNA-Seq dataset of *Nfil3* KO mice fed AL and kept under a light–dark cycle (9). As in *Hlf*/*Dbp*/*Tef* KO mice, clock gene expression and the number of rhythmic liver genes was only slightly affected in the absence of *Nfil3* (Fig. 5*A* and *SI Appendix*, Fig. S6 *A* and *B*). Correspondingly, most rhythmic genes in WT (48%) maintained their temporal expression pattern in both KOs (Fig. 5*B*). Considerably fewer rhythmic genes specifically lost rhythmicity in the respective KO model (13% for *Hlf*/*Dbp*/*Tef* KO and 15% for *Nfil3* KO). Only 5% of rhythmic genes lost oscillatory expression in both KOs (Fig. 5*B*). These results support the hypothesis that NFIL3 can act as a driver of D-box target genes that maintain rhythmicity in *Hlf*/*Dbp*/*Tef* KO mice. In support of this, genes with D-box sites that are bound by DBP or both NFIL3 and DBP tended to be persistently rhythmically expressed across all KOs (Fig. 5*C*). An example of this scenario is the gene *Agpat1* (Fig. 5*D*). Genes with exclusive NFIL3-bound D-boxes in their promoter region, such as *Wee1*, were prone to specifically lose rhythmicity in *Nfil3* KO but still maintained rhythms in *Hlf*/*Dbp*/*Tef* KO mice (Fig. 5 *C* and *E*), further indicating that NFIL3 activity and its target genes are still rhythmic in these KO mice. However, the enrichment of DBP target genes in persistently rhythmic genes, as exemplified for *Glrx* (Fig. 5 *C* and *F*), also showed that NFIL3 alone might be not sufficient to maintain rhythmicity in *Hlf*/*Dbp*/*Tef* KO mice for some genes. These genes were still rhythmic even without binding of NFIL3 to a D-box. Together, *Hlf*/*Dbp*/*Tef* KO mice showed a down-regulation in mean expression levels for many bona fide PARbZip target genes, but rhythms persisted with lower mean expression levels. We hypothesize that NFIL3 is the likely driver for most of these genes with maintained rhythmicity in *Hlf*/*Dbp*/*Tef* KO mice. However, rhythmic NFIL3-independent genes exist,

probably driven directly by the circadian clock as these genes also show direct binding by clock components (Fig. 5*C*).

Discussion

This study provides the *dryR* method, implemented as an R package, to analyze rhythmicity in complex datasets comprising several conditions. We applied *dryR* to analyze newly generated mouse liver RNA-Seq datasets that allow genome-wide comparisons between circadian clock KOs of the positive and negative limb of the core clock loop under controlled feeding cycles. In addition, we also provided a time-resolved RNA-Seq dataset of *Hlf*/*Dbp*/*Tef* KO mice to examine the role of D-box–binding transcription factors for rhythmic gene expression. The analysis of these RNA-Seq datasets demonstrated the versatility of the statistical framework and also provided insights into circadian clock biology. To ease access, we made the RNA-Seq datasets and the statistical analysis available via a web application with an interactive interface (*SI Appendix*, Fig. S8 and https://clockprofile.epfl.ch).

Over the last two decades, many algorithms have been published to identify rhythmically transcribed genes in transcriptomic datasets designed to study circadian rhythms and related phenomena. These time-series transcriptomic datasets are often designed to compare rhythms between conditions (e.g., KO vs. WT or treated vs. untreated conditions). However, approaches designed to assess differential rhythmicity remain rare and are typically designed to test differences between two conditions (34–36). The more general *dryR* algorithm is a parametric model based on generalized harmonic regression and can perform rhythm detection with similar sensitivity and specificity as more specialized methods. In addition, *dryR* allows to simultaneously assess differential rhythmicity and differences in mean levels in more than two conditions. In contrast to other methods that use *P* values to indicate the presence of rhythmicity or differential rhythmicity of a certain feature, *dryR* provides likelihoods for a set of fitted models, which can then be converted to probabilities using established model-selection approaches, such as the Bayesian information criterion (BIC). We note that *dryR* is not designed to provide multiple test-corrected gene sets but is in essence a model-based clustering algorithm, where each gene is assigned to each model (Fig. 1*A*) probabilistically (using BIC weights). In this way, *dryR* can identify the most likely model for each gene expression pattern measured across different conditions and allows comparison of rhythmicity parameters such as mean, phase, and amplitude, which are shared among subsets of conditions. Moreover, although *dryR* was primarily designed for the analysis of RNA-Seq data, its implementation also allows analysis of rhythmic time series assuming normally distributed noise. This includes small-scale datasets, such as metabolite or body temperature measurements, and omics-scale datasets, including microarrays, metabolomics, or proteomics.

Feeding behavior in most mammals follows a pronounced circadian rhythmicity pattern with food mostly consumed during the activity phase (1). Mice are nocturnal animals and consume around 70% of the food during the night (52, 53). In line with others (12, 21, 54, 55), we observed that under a light–dark cycle, the absence of a functional molecular clock dampens rhythms in food intake under an AL paradigm. The loss of a functional SCN master clock in *Bmal1* and *Cry1*/*2* KO mice is likely the main reason for the observed alterations (56, 57). We have seen that these damped rhythms in turn change temporal gene expression in mouse liver. Thus, investigations of transcriptomes in clock-disrupted animal models should be performed under controlled feeding conditions to avoid confounding effects. This conclusion is not restricted to studies with clock-disrupted animal models, as many conditions alter temporal feeding patterns, including high-fat diet (58), calorie restriction (59), stress (60), and age (61).

Restoring the natural feeding rhythms of KO animals by NRF revealed that 33% of rhythmic genes were system-driven and that fewer genes (20%) were direct targets of the cell-autonomous molecular liver clock. Day-restricted feeding is insufficient to completely restore the loss of rhythmic gene expression caused by blunted feeding rhythms in clock-disrupted KO mice (21). In line with our findings, arrhythmic feeding in WT mice blunted the oscillation of the majority of rhythmic liver genes (23, 24). Conspicuously, clock-dependent rhythms had significantly higher amplitudes, which is consistent with our previous analysis of *Bmal1* KOs (27). The number of feeding-dependent rhythmic genes that we observed in our study was higher than in previous reports where 90% of rhythmic genes in the liver are dependent on the cell-autonomous hepatic molecular clock (13, 37). Conversely, the restoration of the cell-autonomous liver clock in *Bmal1* KO mice has been recently shown to rescue only 10% of rhythmic gene expression in the liver (62). This suggests that systemic rhythmic signals generated by hepatocytes can potentially have an impact on the clock in other tissues that, in turn, can feedback on the hepatocyte clock. In that context, clock disruption in hepatocytes reportedly alters rhythmic gene expression in nearby endothelial and Kupffer cells (63). It will be interesting to explore how cell-type–specific circadian clocks communicate with each other in complex tissues.

We observed that both the circadian clock and natural feeding rhythms are key drivers of rhythmic gene expression in the liver. Nevertheless, under a light–dark cycle, a subset of rhythmic liver genes oscillated even in the absence of a functional clock and rhythmic food intake. This observation suggested that clock-independent signals can drive the remaining rhythmicity of those genes, likely involving the SCN. The SCN can receive light signals via the retinohypothalamic tract (64) and, thus, keep a rhythmic activity under a light–dark cycle. Indeed, under a light–dark cycle, both *Cry1*/*2* KO and *Bmal1* KO mice reportedly exhibit rhythmic locomotor activity, which is a known output of the SCN (56, 57). Moreover, the ablation of the SCN attenuates rhythmicity of the liver transcriptome under constant darkness (65). We found that a rhythmic gene cluster of PPARα targets (*SI Appendix*, Fig. S5) and the mTOR signaling pathway (66) show a *Cry1*/*2* KO-specific phase advance that follows the reported advance in SCN activity in *Cry1*/*2* (67). This further supports the idea that SCN-borne signals drive the remaining liver rhythms in the absence of a functional circadian clock and natural feeding cycles. It will be interesting to examine how the SCN conveys rhythmicity to the liver transcriptome. Body temperature cycles might be one route. Indeed, rhythmic body temperature is conserved under constant feeding (24). In addition, we have seen that the temperature-sensitive transcript *Cirbp* (68) and the heat shock protein pathway (69) exhibit rhythmic expression profiles that were conserved across NRF and AL feeding regimens even in the absence of a functional clock. Another possible route is the release of glucocorticoids by the adrenal gland that is also dependent on SCN-borne cues (70, 71), and glucocorticoids have been shown to mediate rhythmic gene expression (29, 72, 73).

The analysis of gene expression in *Hlf*/*Dbp*/*Tef* KO and *Nfil3* KO mice revealed that these clock output factors are involved in the transcriptional regulation of a limited number of genes involved in xenobiotic and lipid metabolism, as already described (39, 74). Surprisingly, PARbZip inactivation has a higher impact on mean expression level than on rhythmicity of the target genes (*SI Appendix*, Fig. S7*F*). This effect on expression levels revisits the role of PARbZip transcription factors in the regulatory landscape of circadian clock-regulated gene expression, identifying factors modulating mean expression levels instead of rhythmicity alone. As an example, while BMAL1 is able to regulate several aspects of xenobiotic detoxification (13), the PARbZip factors amplify this regulation and are required for normal liver detoxification (39). Another interesting finding is the role of the PARbZip factors in the regulation of the bile acid–FXR pathway, which loses rhythmicity in KO mice. While a direct PARbZip regulation has been suggested for example for *Cyp7a1* (75), we did

not detect binding of PARbZip transcription factors near the promoters of this gene in published ChIP-Seq datasets (9). The entire detoxification pathway is also regulated by bile acids (76). Bile acid elimination is controlled by the xenobiotic receptors PXR and CAR (77). Therefore, an indirect regulation through the deficient rhythmic elimination of bile acids is an alternative mechanism.

While our study has focused on the transcriptional regulation of circadian physiology, posttranscriptional (78) and posttranslational (79) regulation is equally important. Thus, future omics-scale investigations on the posttranscriptional and posttranslational level would be desirable and could provide more mechanistic insights into the role of feeding cycles and the circadian clock network on liver physiology. Overall, combining a powerful analysis framework with a comprehensive dataset of several clock KO models under controlled feeding regimens provides an integrated view on how the clock network and feeding cues work together in concert to drive rhythmic gene expression in the liver.

Materials and Methods

Details about the described procedures and data analysis are available at *SI Appendix*, *SI Materials and Methods*.

Mouse Experiments. Male mice were kept under a 12-h light–12-h dark cycle. All mice used in the experiments were between 9 to 14 wk old. The generation of *Bmal1* and *Cry1/2* KO mice have been previously described (57, 66). Four days before sacrifice, *Bmal1* and *Cry1/2* KO mice had either free access to chow food (ad libitum [AL]) or only during the dark phase (night restricted feeding [NRF]). The generation of *Hlf/Dbp/Tef* KO mice has been already described (48). These animals were fed AL as feeding rhythms were not different from WT siblings (Fig. 4*B*). Mice were killed, and livers were dissected, snap-frozen in liquid nitrogen, and stored at −80 °C until further processing. The studies were conducted in accordance with the regulations of the veterinary office of the Canton of Vaud (experiments conducted at Nestlé Research) and Geneva (experiments conducted at University of Geneva).

Food-Intake Measurements. *Bmal1* and *Cry1/2* KO mice were kept single-housed in phenotyping cages (TSE Systems) under a 12-h light/12-h dark cycle with an NRF and AL regimen as previously described (80). Food intake was measured every 15 min. Feeding frequency for *Hlf/Dbp/Tef* KO mice and WT littermates was measured as previously described (81).

RNA Extraction and RNA-Seq. RNA extraction was performed as described (82). Libraries were prepared using the TruSeq Stranded mRNA Library Prep kit (Illumina) and sequenced on a HiSeq2500 or NextSeq500 (Illumina).

Data Availability. Raw files and technical details about the RNA-Seq data have been deposited in NCBI's Gene Expression Omnibus (83) and are accessible through GEO Series accession nos. GSE135898 and GSE135875. The *DryR* code is available in GitHub at https://github.com/naef-lab/dryR. Results and visualization are available at https://clockprofile.epfl.ch.

ACKNOWLEDGMENTS. We thank Ueli Schibler for the utilization of PARbZip KO mouse data and Gijsbertus van der Horst for providing *Cry1/2* KO mice. We thank José-Luis Sanchez-Garcia for technical support and Jake Yeung for providing insightful discussions. This work was supported by the European Research Council through individual Starting Grant ERC-2010-StG-260988 (to F.G.). F.G. receives support from the Institute for Molecular Bioscience, The University of Queensland. F.N. is supported by Swiss National Science Foundation Grant 310030_173079 and the Ecole Polytechnique Fédérale de Lausanne (EPFL). We thank Frederic Raymond and Sylviane Metairon from Nestlé Research and Bastien Mangeat and Lionel Ponsonnet from the Gene Expression Core Facility at EPFL for high-throughput sequencing.

1. F. Atger, D. Mauvoisin, B. Weger, C. Gobet, F. Gachon, Regulation of mammalian physiology by interconnected circadian and feeding rhythms. *Front. Endocrinol. (Lausanne)* **8**, 42 (2017).
2. F. Rijo-Ferreira, J. S. Takahashi, Genomics of circadian rhythms in health and disease. *Genome Med.* **11**, 82 (2019).
3. M. Astiz, I. Heyde, H. Oster, Mechanisms of communication in the mammalian circadian timing system. *Int. J. Mol. Sci.* **20**, 343 (2019).
4. U. Schibler *et al.*, Clock-talk: Interactions between central and peripheral circadian oscillators in mammals. *Cold Spring Harb. Symp. Quant. Biol.* **80**, 223–232 (2015).
5. J. S. Takahashi, Transcriptional architecture of the mammalian circadian clock. *Nat. Rev. Genet.* **18**, 164–179 (2017).
6. N. Preitner *et al.*, The orphan nuclear receptor REV-ERBalpha controls circadian transcription within the positive limb of the mammalian circadian oscillator. *Cell* **110**, 251–260 (2002).
7. T. K. Sato *et al.*, A functional genomics strategy reveals Rora as a component of the mammalian circadian clock. *Neuron* **43**, 527–537 (2004).
8. F. Gachon, Physiological function of PARbZip circadian clock-controlled transcription factors. *Ann. Med.* **39**, 562–571 (2007).
9. H. Yoshitane *et al.*, Functional D-box sequences reset the circadian clock and drive mRNA rhythms. *Commun. Biol.* **2**, 300 (2019).
10. J. Mermet, J. Yeung, F. Naef, Systems chronobiology: Global analysis of gene regulation in a 24-hour periodic world. *Cold Spring Harb. Perspect. Biol.* **9**, a028720 (2017).
11. H. Reinke, G. Asher, Crosstalk between metabolism and circadian clocks. *Nat. Rev. Mol. Cell Biol.* **20**, 227–241 (2019).
12. K. A. Lamia, K. F. Storch, C. J. Weitz, Physiological significance of a peripheral tissue circadian clock. *Proc. Natl. Acad. Sci. U.S.A.* **105**, 15172–15177 (2008).
13. B. P. Johnson *et al.*, Hepatocyte circadian clock controls acetaminophen bioactivation through NADPH-cytochrome P450 oxidoreductase. *Proc. Natl. Acad. Sci. U.S.A.* **111**, 18757–18762 (2014).
14. E. E. Zhang *et al.*, Cryptochrome mediates circadian regulation of cAMP signaling and hepatic gluconeogenesis. *Nat. Med.* **16**, 1152–1156 (2010).
15. I. Schmutz, J. A. Ripperger, S. Baeriswyl-Aebischer, U. Albrecht, The mammalian clock component PERIOD2 coordinates circadian output by interaction with nuclear receptors. *Genes Dev.* **24**, 345–357 (2010).
16. K. A. Lamia *et al.*, Cryptochromes mediate rhythmic repression of the glucocorticoid receptor. *Nature* **480**, 552–556 (2011).
17. B. Grimaldi *et al.*, PER2 controls lipid metabolism by direct regulation of PPARγ. *Cell Metab.* **12**, 509–520 (2010).
18. K. Nagai, T. Nishio, H. Nakagawa, S. Nakamura, Y. Fukuda, Effect of bilateral lesions of the suprachiasmatic nuclei on the circadian rhythm of food-intake. *Brain Res.* **142**, 384–389 (1978).
19. F. K. Stephan, I. Zucker, Circadian rhythms in drinking behavior and locomotor activity of rats are eliminated by hypothalamic lesions. *Proc. Natl. Acad. Sci. U.S.A.* **69**, 1583–1586 (1972).
20. M. Hatori *et al.*, Time-restricted feeding without reducing caloric intake prevents metabolic diseases in mice fed a high-fat diet. *Cell Metab.* **15**, 848–860 (2012).
21. C. Vollmers *et al.*, Time of feeding and the intrinsic circadian clock drive rhythms in hepatic gene expression. *Proc. Natl. Acad. Sci. U.S.A.* **106**, 21453–21458 (2009).
22. F. Damiola *et al.*, Restricted feeding uncouples circadian oscillators in peripheral tissues from the central pacemaker in the suprachiasmatic nucleus. *Genes Dev.* **14**, 2950–2961 (2000).
23. F. Mange *et al.*; CycliX Consortium, Diurnal regulation of RNA polymerase III transcription is under the control of both the feeding-fasting response and the circadian clock. *Genome Res.* **27**, 973–984 (2017).
24. B. J. Greenwell *et al.*, Rhythmic food intake drives rhythmic gene expression more potently than the hepatic circadian clock in mice. *Cell Rep.* **27**, 649.e645–657.e645 (2019).
25. M. E. Hughes *et al.*, Guidelines for genome-scale analysis of biological rhythms. *J. Biol. Rhythms* **32**, 380–393 (2017).
26. J. Yeung, F. Naef, Rhythms of the genome: Circadian dynamics from chromatin topology, tissue-specific gene expression, to behavior. *Trends Genet.* **34**, 915–926 (2018).
27. J. Yeung *et al.*, Transcription factor activity rhythms and tissue-specific chromatin interactions explain circadian gene expression across organs. *Genome Res.* **28**, 182–191 (2018).
28. B. D. Weger *et al.*, The mouse microbiome is required for sex-specific diurnal rhythms of gene expression and metabolism. *Cell Metab.* **29**, 362.e8–382.e8 (2019).
29. B. D. Weger *et al.*, Extensive regulation of diurnal transcription and metabolism by glucocorticoids. *PLoS Genet.* **12**, e1006512 (2016).
30. C. R. Cederroth *et al.*, Circadian regulation of cochlear sensitivity to noise by circulating glucocorticoids. *Curr. Biol.* **29**, 2477–2487.e6 (2019).
31. V. Petrenko *et al.*, Pancreatic α- and β-cellular clocks have distinct molecular properties and impact on islet hormone secretion and gene expression. *Genes Dev.* **31**, 383–398 (2017).
32. F. Atger *et al.*, Circadian and feeding rhythms differentially affect rhythmic mRNA transcription and translation in mouse liver. *Proc. Natl. Acad. Sci. U.S.A.* **112**, E6579–E6588 (2015).
33. R. S. Pulido *et al.*, Neuronal activity regulates blood-brain barrier efflux transport through endothelial circadian genes. *Neuron* **108**, 937–952.e7 (2020).
34. R. Parsons, R. Parsons, N. Garner, H. Oster, O. Rawashdeh, CircaCompare: A method to estimate and statistically support differences in mesor, amplitude and phase, between circadian rhythms. *Bioinformatics* **36**, 1208–1212 (2020).
35. P. F. Thaben, P. O. Westermark, Differential rhythmicity: Detecting altered rhythmicity in biological data. *Bioinformatics* **32**, 2800–2808 (2016).
36. J. M. Singer, J. J. Hughey, LimoRhyde: A flexible approach for differential analysis of rhythmic transcriptome data. *J. Biol. Rhythms* **34**, 5–18 (2019).

37. B. Kornmann, O. Schaad, H. Bujard, J. S. Takahashi, U. Schibler, System-driven and oscillator-dependent circadian transcription in mice with a conditionally active liver clock. *PLoS Biol.* **5**, e34 (2007).
38. D. Druzd *et al*., Lymphocyte circadian clocks control lymph node trafficking and adaptive immune responses. *Immunity* **46**, 120–132 (2017).
39. F. Gachon, F. F. Olela, O. Schaad, P. Descombes, U. Schibler, The circadian PAR-domain basic leucine zipper transcription factors DBP, TEF, and HLF modulate basal and inducible xenobiotic detoxification. *Cell Metab.* **4**, 25–36 (2006).
40. Y. Wang *et al*., A proteomics landscape of circadian clock in mouse liver. *Nat. Commun.* **9**, 1553 (2018).
41. J. A. Sobel *et al*.; CycliX consortium, Transcriptional regulatory logic of the diurnal cycle in the mouse liver. *PLoS Biol.* **15**, e2001069 (2017).
42. L. Canaple *et al*., Reciprocal regulation of brain and muscle Arnt-like protein 1 and peroxisome proliferator-activated receptor alpha defines a novel positive feedback loop in the rodent liver circadian clock. *Mol. Endocrinol.* **20**, 1715–1727 (2006).
43. J. Wang *et al*., Nuclear proteomics uncovers diurnal regulatory landscapes in mouse liver. *Cell Metab.* **25**, 102–117 (2017).
44. C. Crumbley, Y. Wang, D. J. Kojetin, T. P. Burris, Characterization of the core mammalian clock component, NPAS2, as a REV-ERBalpha/RORalpha target gene. *J. Biol. Chem.* **285**, 35386–35392 (2010).
45. J. E. Baggs *et al*., Network features of the mammalian circadian clock. *PLoS Biol.* **7**, e52 (2009).
46. H. Cho *et al*., Regulation of circadian behaviour and metabolism by REV-ERB-α and REV-ERB-β. *Nature* **485**, 123–127 (2012).
47. N. Koike *et al*., Transcriptional architecture and chromatin landscape of the core circadian clock in mammals. *Science* **338**, 349–354 (2012).
48. F. Gachon *et al*., The loss of circadian PAR bZip transcription factors results in epilepsy. *Genes Dev.* **18**, 1397–1412 (2004).
49. J. Y. Chiang, R. Kimmel, C. Weinberger, D. Stroup, Farnesoid X receptor responds to bile acids and represses cholesterol 7alpha-hydroxylase gene (CYP7A1) transcription. *J. Biol. Chem.* **275**, 10918–10924 (2000).
50. F. Sinturel *et al*., Diurnal oscillations in liver mass and cell size accompany ribosome assembly cycles. *Cell* **169**, 651.e614–663.e614 (2017).
51. S. Mitsui, S. Yamaguchi, T. Matsuo, Y. Ishida, H. Okamura, Antagonistic role of E4BP4 and PAR proteins in the circadian oscillatory mechanism. *Genes Dev.* **15**, 995–1006 (2001).
52. M. Kurokawa, K. Akino, K. Kanda, A new apparatus for studying feeding and drinking in the mouse. *Physiol. Behav.* **70**, 105–112 (2000).
53. K. S. Gannon, J. C. Smith, R. Henderson, P. Hendrick, A system for studying the microstructure of ingestive behavior in mice. *Physiol. Behav.* **51**, 515–521 (1992).
54. Y. Adamovich *et al*., Circadian clocks and feeding time regulate the oscillations and levels of hepatic triglycerides. *Cell Metab.* **19**, 319–330 (2014).
55. F. W. Turek *et al*., Obesity and metabolic syndrome in circadian Clock mutant mice. *Science* **308**, 1043–1045 (2005).
56. M. K. Bunger *et al*., Mop3 is an essential component of the master circadian pacemaker in mammals. *Cell* **103**, 1009–1017 (2000).
57. G. T. van der Horst *et al*., Mammalian Cry1 and Cry2 are essential for maintenance of circadian rhythms. *Nature* **398**, 627–630 (1999).
58. A. Kohsaka *et al*., High-fat diet disrupts behavioral and molecular circadian rhythms in mice. *Cell Metab.* **6**, 414–421 (2007).
59. V. A. Acosta-Rodriguez, M. H. M. de Groot, F. Rijo-Ferreira, C. B. Green, J. S. Takahashi, Mice under caloric restriction self-impose a temporal restriction of food intake as revealed by an automated feeder system. *Cell Metab.* **26**, 267–277.e262 (2017).
60. S. Z. Jiang, L. E. Eiden, Activation of the HPA axis and depression of feeding behavior induced by restraint stress are separately regulated by PACAPergic neurotransmission in the mouse. *Stress* **19**, 374–382 (2016).
61. C. Yamada, S. Mogami, T. Hattori, Psychological stress exposure to aged mice causes abnormal feeding patterns with changes in the bout number. *Aging (Albany NY)* **9**, 2269–2287 (2017).
62. K. B. Koronowski *et al*., Defining the independence of the liver circadian clock. *Cell* **177**, 1448.e14–1462.e14 (2019).
63. D. Guan *et al*., The hepatocyte clock and feeding control chronophysiology of multiple liver cell types. *Science* **369**, 1388–1394 (2020).
64. M. H. Hastings, E. S. Maywood, M. Brancaccio, Generation of circadian rhythms in the suprachiasmatic nucleus. *Nat. Rev. Neurosci.* **19**, 453–469 (2018).
65. R. A. Akhtar *et al*., Circadian cycling of the mouse liver transcriptome, as revealed by cDNA microarray, is driven by the suprachiasmatic nucleus. *Curr. Biol.* **12**, 540–550 (2002).
66. C. Jouffe *et al*., The circadian clock coordinates ribosome biogenesis. *PLoS Biol.* **11**, e1001455 (2013).
67. H. Albus *et al*., Cryptochrome-deficient mice lack circadian electrical activity in the suprachiasmatic nuclei. *Curr. Biol.* **12**, 1130–1133 (2002).
68. J. Morf *et al*., Cold-inducible RNA-binding protein modulates circadian gene expression posttranscriptionally. *Science* **338**, 379–383 (2012).
69. H. Reinke *et al*., Differential display of DNA-binding proteins reveals heat-shock factor 1 as a circadian transcription factor. *Genes Dev.* **22**, 331–345 (2008).
70. R. M. Buijs *et al*., Anatomical and functional demonstration of a multisynaptic suprachiasmatic nucleus adrenal (cortex) pathway. *Eur. J. Neurosci.* **11**, 1535–1544 (1999).
71. A. Ishida *et al*., Light activates the adrenal gland: Timing of gene expression and glucocorticoid release. *Cell Metab.* **2**, 297–307 (2005).
72. K. Oishi *et al*., Genome-wide expression analysis reveals 100 adrenal gland-dependent circadian genes in the mouse liver. *DNA Res.* **12**, 191–202 (2005).
73. A. B. Reddy *et al*., Glucocorticoid signaling synchronizes the liver circadian transcriptome. *Hepatology* **45**, 1478–1488 (2007).
74. F. Gachon *et al*., Proline- and acidic amino acid-rich basic leucine zipper proteins modulate peroxisome proliferator-activated receptor alpha (PPARalpha) activity. *Proc. Natl. Acad. Sci. U.S.A.* **108**, 4794–4799 (2011).
75. D. J. Lavery, U. Schibler, Circadian transcription of the cholesterol 7 alpha hydroxylase gene may involve the liver-enriched bZIP protein DBP. *Genes Dev.* **7**, 1871–1884 (1993).
76. B. Goodwin *et al*., A regulatory cascade of the nuclear receptors FXR, SHP-1, and LRH-1 represses bile acid biosynthesis. *Mol. Cell* **6**, 517–526 (2000).
77. M. Wagner *et al*., CAR and PXR agonists stimulate hepatic bile acid and bilirubin detoxification and elimination pathways in mice. *Hepatology* **42**, 420–430 (2005).
78. J. Wang *et al*., Circadian clock-dependent and -independent posttranscriptional regulation underlies temporal mRNA accumulation in mouse liver. *Proc. Natl. Acad. Sci. U.S.A.* **115**, E1916–E1925 (2018).
79. D. Mauvoisin, F. Gachon, Proteomics in circadian biology. *J. Mol. Biol.* **432**, 3565–3577 (2020).
80. C. Jouffe *et al*., Perturbed rhythmic activation of signaling pathways in mice deficient for Sterol Carrier Protein 2-dependent diurnal lipid transport and metabolism. *Sci. Rep.* **6**, 24631 (2016).
81. S. A. Brown, G. Zumbrunn, F. Fleury-Olela, N. Preitner, U. Schibler, Rhythms of mammalian body temperature can sustain peripheral circadian clocks. *Curr. Biol.* **12**, 1574–1583 (2002).
82. E. E. Schmidt, U. Schibler, Cell size regulation, a mechanism that controls cellular RNA accumulation: Consequences on regulation of the ubiquitous transcription factors Oct1 and NF-Y and the liver-enriched transcription factor DBP. *J. Cell Biol.* **128**, 467–483 (1995).
83. R. Edgar, M. Domrachev, A. E. Lash, Gene Expression Omnibus: NCBI gene expression and hybridization array data repository. *Nucleic Acids Res.* **30**, 207–210 (2002).